Fuel 350 (2023) 128787

Contents lists available at ScienceDirect

Fuel

journal homepage: www.elsevier.com/locate/fuel

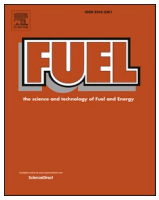

Full Length Article

Study on initiation characteristics of oblique detonation induced by hydrogen jets in acetylene-air mixtures

Zhang Yichen [a], Xiang Gaoxiang [a,d,e,*], Gao Xiang [b], Yu Jia [a], Hu Xiquan [a], Xin Yirong [a], Li Danyang [a], Wang Qiu [c]

[a] School of Mechanics, Civil Engineering & Architecture, Northwestern Polytechnical University, Xi'an 710129, China
[b] College of Geology and Environment, Xi'an University of Science and Technology, Xi'an 710054, China
[c] State Key Laboratory of High Temperature Gas Dynamics, Institute of Mechanics, Chinese Academy of Sciences, Beijing 100190, China
[d] Research & Development Institute of Northwestern Polytechnical University in Shenzhen, Shenzhen 518057, China
[e] Innovation Center NPU Chongqing, Northwestern Polytechnical University, Chongqing, 400000, China

ARTICLE INFO

Keywords:
Oblique detonation wave
Acetylene
Transverse jet
Numerical simulation

ABSTRACT

In this paper, effects of hydrogen jets in acetylene-air mixtures on the initiation characteristics of oblique detonation wave (ODW) are investigated, the two-dimensional (2D) multi-component NS equations considering detailed chemical reactions are solved. Influences of the transverse jet on flow field characteristics of the ODW are studied, including the initiation characteristics, the wave structures, and the state parameters. The existence of the jet changes the ignited mode of the ODW from double Mach interaction to single Mach interaction. Several wave configurations and their transitions induced by the jets are observed, including deflagration-to-detonation transition (DDT), jet-induced bow shock wave (BSW) in front of the transverse jet and rapidly develops into ODW, and ODW that generated directly in front of the transverse jet. The structure of these three wave systems is mainly influenced by the flow discharge of the hydrogen jet. When the hydrogen jet is small, no combustion is induced by the BSW in front of the jet. ODW is induced by the action of the deflagration wave and OSW. Increasing the hydrogen jet, BSW induces combustion and rapidly develops into ODW. When the hydrogen jet is large enough, the BSW disappears and direct detonation combustion occurs to produce ODW. Two types of relationships are obtained between the initiated position and the position of the transverse jet: the U-shaped curve at low flow discharge and the positive correlation at high flow discharge. When the flow discharge is small and no shock wave-induced combustion occurs, the initiated position is influenced by the position of the deflagration wave interacting with the OSW, which forms a U-shaped curve with the position of hydrogen jet. When the flow discharge is high and shock wave induced combustion occurs, ODW is rapidly developed behind the jet, resulting in a positive correlation between the initiated position and the position of hydrogen jet. Furthermore, the viscous effect has significant influence on the flow field characteristics of ODW, it promotes the transition between these initiation modes and shortens the initiation distance of oblique detonation. The findings of this study can better help understand the effect of transverse hydrogen jets on ODW initiation and contribute to theoretical studies and engineering applications of oblique detonation engines.

1. Introduction

Detonation is a highly efficient form of combustion with significant potential applications in hypersonic propulsion [1,2]. There are three types of detonation engines: pulse detonation engines (PDE) [3,4], rotating detonation engines (RDE), and oblique detonation engines (ODE) [5,6]. Hydrogen and hydrocarbon fuels are widely used in the field of aerospace propulsion, especially in the research of gaseous detonation. The oblique detonation engine (ODE) is a type of ramjet engine that is based on the ODW and is suitable for air-breathing hypersonic aircraft [7]. It has the advantages of wide flight Mach number range, low flight resistance, simple structure, and light weight [8–14].

Researchers have conducted extensive research on the wave system structure, transition characteristics, and stationary characteristics of ODW in recent decades [15–26]. Li determined the wave structure of the ODW in their numerical simulations, it consists of the oblique shock wave (OSW), the induction zone, deflagration waves, and the ODW

* Corresponding author at: School of Mechanics, Civil Engineering & Architecture, Northwestern Polytechnical University, Xi'an 710129, China.
E-mail address: xianggx@nwpu.edu.cn (X. Gaoxiang).

https://doi.org/10.1016/j.fuel.2023.128787
Received 4 December 2022; Received in revised form 9 March 2023; Accepted 21 May 2023
Available online 1 June 2023

Nomenclature

T_0	initial temperature	T	temperature
P_0	initial pressure	h	specific enthalpy
M	Mach number	R_0	universal gas constant
U	conservation variable vector	ω	molecular weight
F	convective flux vector in x-direction	q_x	heat flow capacity in x-direction
G	convective flux vector in y-direction	q_y	heat flow capacity in y-direction
S	source item vector	k	thermal conductivity coefficient
F_v	viscous flux vector in x-direction	c_p	specific heat
G_v	viscous flux vector in y-direction	Pr	Prandtl number
τ	shear stress	μ	viscosity coefficient
u	velocity in x-direction	L_J	position of jet nozzle
v	velocity in y-direction	L_S	length of oblique shock wave
ρ	density	R_i	gas constant of species i
p	pressure	c_{pi}	constant pressure specific heat of species i
		Y_i	mass fraction of species i
		W_i	mole mass of species i

[15]. Following that, Viguier, Desbordes, and Kamel et al. performed experiments to determine the structure of the ODW, confirming the accuracy of Li's numerical simulation [16–18]. Teng and Miao discovered that there are two types of transitions from the OSW to the ODW: the smooth transition and the abrupt transition [19,20]. Yang discovered that as the Mach number increases, the initial position of oblique detonation moves upstream, and the transition form changes from abrupt transition to smooth transition [21]. According to Liu's research, there are two types of hysteresis in ODWs: upstream–downstream triple point hysteresis and smooth-abrupt pattern hysteresis [22]. Fang and Chen investigated the effect of equivalence ratio on the initiation of oblique detonation and discovered that the equivalence ratio which is too high or too low is not conducive to the initiation of oblique detonation [23,24]. Qin and Xiang investigated the structural evolution of ODWs in confined spaces, especially the effects of expansion and compression waves [25,26].

The wedge induced ODW has the disadvantages of long initiation distance and is easy to result in the failure of oblique detonation. External assistance should be considered to speed up the initiation of the ODW and obtain a steady ODW. In the recent years, many studies have examined the use of extra jets to improve the initiation of the ODW [3,27–32]. Qin investigated the effect of co-flow hot jets on the initiation of an ODW and discovered that the strength of the first and second jet shock waves is greater than that of the leading shock wave, resulting in a significant reduction in the initiation length of the ODW [27]. Cheng presented a new approach for facilitating the creation of the precursor shock wave and the flame propagation speed in a deflagration wave in a stoichiometric methane-oxygen mixture utilizing a non-reactive gas jet [28]. According to Wang's research, the hot jet with larger strength was more favorable to detonation initiation [29]. According to Li's research, the transition from inert OSW to ODW occurs precisely near the position of hot jet injection, and consequently the length of the combustor can be reduced [30]. Additionally, there are other studies that have found similar conclusions [31,32]. In the numerical simulation research, due to the hydrogen chemical reaction model is simple and can save a lot of time and computing resources, most investigations of the ODW are based on hydrogen-air mixtures [33,34]. However, in practical engineering, because of the high reaction sensitivity of hydrogen, it is easy to cause safety problems. Hydrogen as a fuel has many disadvantages, such as storage and transportation difficulties [35]. Therefore, based on hydrogen fuel, researchers have studied the ODW induced by many other fuels, such as hydrocarbon fuels and kerosene. [36–42]. Fang and Zhang studied the ODW induced by acetylene and observed the initiation characteristics and wave structure of ODW in acetylene-oxygen mixture under argon dilution [36,37]. Zhang simulated that the detonation wave in methane propagates in six different modes in tubes of varying diameters, and he conducted experimental research on the relationship between the detonation limit and cell size [38–41]. Furthermore, due to hydrogen's activity, it had been added in the fuel–air mixture to examine the detonation wave [4,42]. According to Xi's findings, adding hydrogen to methane can shorten the length of the induction zone. And when the hydrogen content increases, the initiation length decreases nonlinearly [42]. Fig. 1 presents the general sketch of the problem under study. Therefore, in this paper, the ODW induced by hydrogen jets in acetylene-air mixtures is investigated in conjunction with previous studies, and the accelerated initiation of ODW is achieved by hydrogen jets.

In this paper, numerical studies on oblique detonation induced by hydrogen jets in acetylene-air mixtures are performed. Based on the detailed chemical reaction, the effects of transverse jet on the oblique detonation initiation of premixed acetylene-air mixture are studied by solving the two-dimensional Navier-Stokes equation. In this paper, three wave structures of ODWs in acetylene-air mixture under hydrogen jet were observed, two relationships between the initiation position and

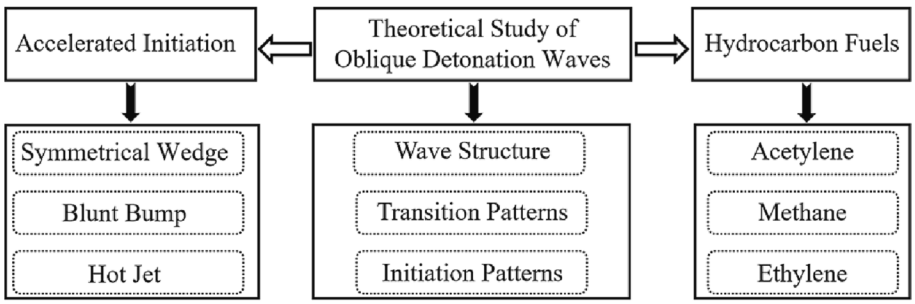

Fig. 1. General sketch of the problem under study.

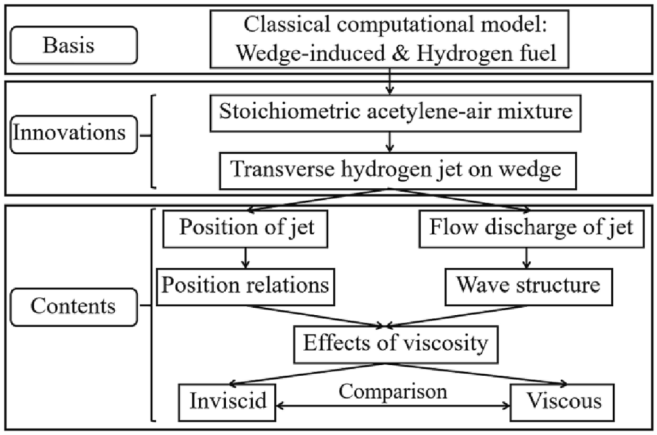

Fig. 2. The specific workflow.

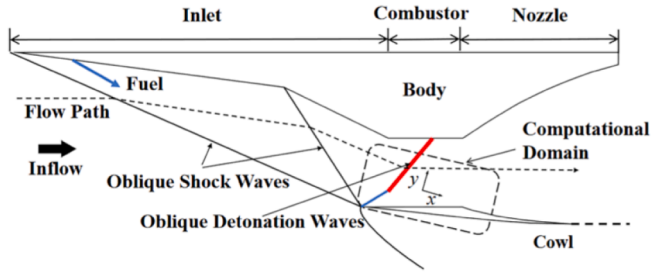

(a)Schematic of ODE

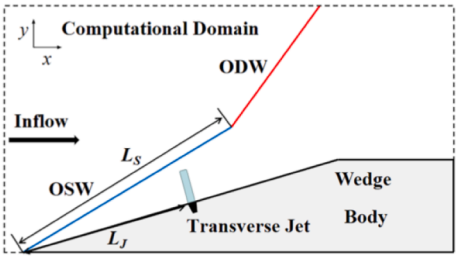

(b)Computational domain and coordinate system

Fig. 3. Schematic.

transverse jet were obtained, and the influence of viscous effect was studied. First, the ODW induced by hydrogen jets with different flow rates and positions are numerically simulated in inviscid conditions. Second, the numerical simulations are performed in viscous conditions. Finally, the obtained simulation results are analyzed and discussed. As shown in Fig. 2, the specific workflow is compiled into a flowchart. Section 2 introduces the mathematical and physical model. Section 3 investigates the effects of the transverse jet on oblique detonation, including the position and flow discharge of the transverse jet, the viscous effects. Section 4 gives the conclusion of this paper.

2. Physical and mathematical models

Fig. 3 shows the schematic of ODE (a) and the computational domain and coordinate system (b). As is shown in Fig. 3(a), the ODE consists of three parts: the inlet, the combustor, and the nozzle. First, the inflow and fuel are sufficiently mixed in the inlet and compressed by two OSWs. Then, the wedge of the combustor induces the OSW, it causes a high post-shock temperature and makes the chemical reaction occur, results in the formation of ODW. The specific computational domain is presented in Fig. 3(b). The solid black line represents the wall of the combustor, which has a transverse jet nozzle. In Section 3.1, viscosity is not considered, and the wall condition is set to slip boundary condition. In Section 3.2, on the other hand, viscosity is considered, and the wall condition is set to non-slip boundary condition. The inflow air comes from the left, so the dashed line on the left is set as the inflow conditions. According to the flow trajectory, the mixed gas flows out to the above and right boundaries, so the dashed lines on the top are far-field condition and the right are set as outflow conditions.

In this paper, the flight Mach number is $M_0 = 9$. Flight conditions are standard atmospheric parameters at an altitude of 30 km ($T_0 = 226.51$ K, $P_0 = 1197$ Pa). The incoming gas is a well-mixed acetylene-air mixture. Among them, the stoichiometric ratio of acetylene, oxygen and nitrogen is 0.4:1:3.76. Two 9° wedges in the inlet compress the premixed flow before it enters the combustor. According to the oblique shock relationship, after the inflow is compressed twice in the inlet, the temperature and pressure of the inflow at the combustor are $T = 618$ K, $P = 22380$ Pa. In addition, the angle between the wedge and the inflow is 18°. The direction of the transverse jet is vertical to the wedge surface, and the width of the jet nozzle is fixed at 2 mm. In this paper, the velocity of the transverse jet is set to Mach 1, and the total temperature of the transverse jet is fixed at 300 K. The total pressure of the transverse jet is not fixed, 50 KPa, 100 KPa, 200 KPa and 300 KPa are calculated as needed. In this paper, the length of the computational domain in × direction is 250 mm, while the length in *y* direction is 150 mm. The length of the wedge is 200 mm, and the distance from the front end of the wedge to the jet nozzle is denoted as L_J. To compare the initiation positions of ODW under different conditions, the length of OSW is denoted as L_S.

In this paper, the two-dimensional multi-component Navier-Stokes equations considering elementary reactions are solved, i.e.:

$$\frac{\partial U}{\partial t}+\frac{\partial F}{\partial x}+\frac{\partial G}{\partial y}=\frac{\partial F_v}{\partial x}+\frac{\partial G_v}{\partial y}+S \tag{1}$$

where U is conservation variable vector, F and F_v are convective flux vector and viscous flux vector in x-direction, G and G_v are convective flux vector and viscous flux vector in y-direction, and S is source item vector. Each vector is specified as follows:

$$U=\begin{Bmatrix}\rho_1\\ \vdots\\ \rho_n\\ \rho u\\ \rho v\\ e\end{Bmatrix}, F=\begin{Bmatrix}\rho_1 u\\ \vdots\\ \rho_n u\\ \rho u^2+p\\ \rho uv\\ (e+p)u\end{Bmatrix}, G=\begin{Bmatrix}\rho_1 v\\ \vdots\\ \rho_n v\\ \rho uv\\ \rho v^2+p\\ (e+p)v\end{Bmatrix}, S=\begin{Bmatrix}\dot{\omega}_1\\ \vdots\\ \dot{\omega}_n\\ 0\\ 0\\ 0\end{Bmatrix} \tag{2}$$

$$F_v=\begin{Bmatrix}0\\ \vdots\\ 0\\ \tau_{xx}\\ \tau_{xy}\\ u\tau_{xx}+v\tau_{xy}-q_x\end{Bmatrix}, G_v=\begin{Bmatrix}0\\ \vdots\\ 0\\ \tau_{yx}\\ \tau_{yy}\\ u\tau_{yx}+v\tau_{yy}-q_y\end{Bmatrix}, \tag{3}$$

$$\begin{bmatrix}\tau_{xx} & \tau_{xy}\\ \tau_{yx} & \tau_{yy}\end{bmatrix}=\mu\begin{bmatrix}\frac{4}{3}\frac{\partial u}{\partial x}-\frac{2}{3}\frac{\partial v}{\partial y} & \frac{\partial u}{\partial y}+\frac{\partial v}{\partial x}\\ \frac{\partial u}{\partial y}+\frac{\partial v}{\partial x} & \frac{4}{3}\frac{\partial v}{\partial y}-\frac{2}{3}\frac{\partial u}{\partial x}\end{bmatrix}, \tag{4}$$

In equation (2), the subscript i (i = 1,2… n) refers to the i-th substances. The total specific energy e and total density ρ can be determined by

$$\rho=\sum_{i=1}^{n}\rho_i,\quad e=\rho h-p+\frac{1}{2}\rho(u^2+v^2) \tag{5}$$

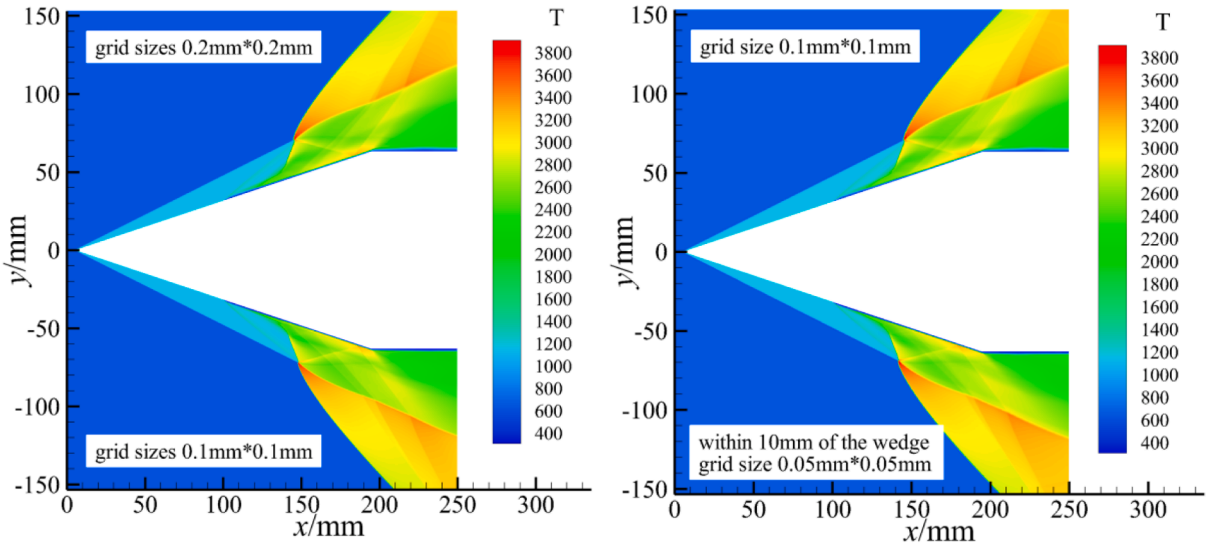

(a)Double mesh refinement (b) Partial mesh refinement

Fig. 4. Temperature field of the ODW at different grid sizes.

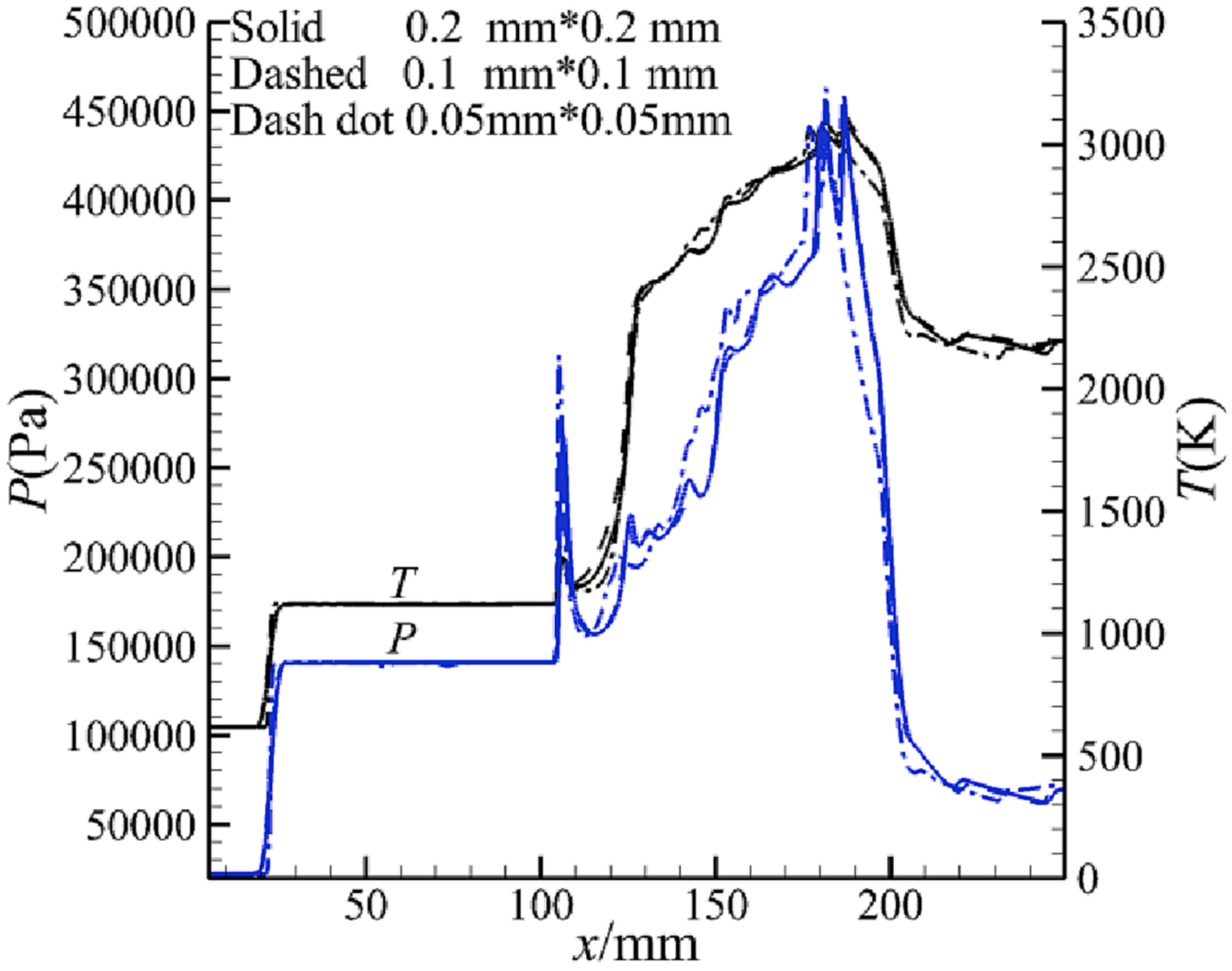

Fig. 5. Temperature and pressure curve at different grid sizes.

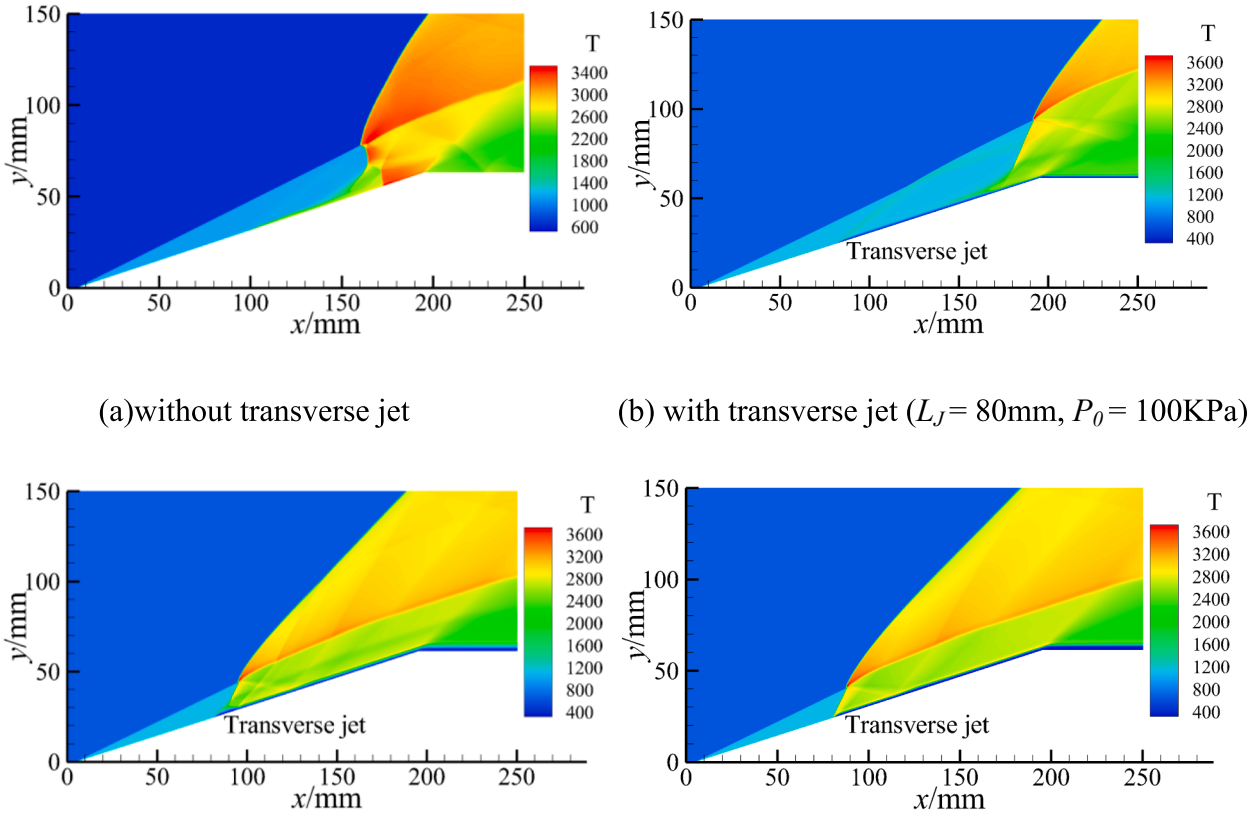

(a)without transverse jet (b) with transverse jet (L_J= 80mm, P_0= 100KPa)

(c)with transverse jet (L_J= 80mm, P_0= 200KPa) (d)with transverse jet (L_J= 80mm, P_0= 300KPa)

Fig. 6. Temperature field of ODW at different conditions.

where u is the velocity in the x-direction and v is the velocity in the y-direction. h is the specific enthalpy, which is defined as $h = \sum_{i=1}^{n} \rho_i h_i / \rho$. The equation of state is $p = \sum_{i=1}^{n} \rho_i \frac{R_0}{\omega_i} T$, R_0 is the gas constant, and ω_i is the molecular weight of the i-th species.

In equation (3), τ represents shear stress, and q_x and q_y represent the components of heat flow in two coordinate directions, which can be expressed as

$$q_x = -k\frac{\partial T}{\partial x}, \quad q_y = k\frac{\partial T}{\partial y} \tag{6}$$

where k is the thermal conductivity coefficient, and the calculation formula is $k = \frac{\mu \cdot c_p}{Pr}$. Pr is the Prandtl number, here Pr = 0.72. The viscosity coefficient is $\mu = 1.458 \times 10^{-6} \frac{T^{3/2}}{T+111}$, given by Sutherland formula. c_p is the specific heat at constant pressure, and the calculation formula is $c_p = \sum_{i=1}^{ns} Y_i c_{pi}$, where Y_i is the mass fraction of species i and c_{pi} is the constant pressure specific heat of species i. c_{pi} is expressed as a function of temperature T through NASA's empirical formula [43], which is calculated as

$$\frac{c_{pi}(T)}{R_i} = a_{i1} + a_{i2}T + a_{i3}T^2 + a_{i4}T^3 + a_{i5}T^4 \tag{7}$$

where the coefficients a_{i1} - a_{i5} are available from the literature [43]. R_i is the gas constant of species i, which is given by the universal gas constant R_0 = 8.314 J/(mol·K) and W_i is mole mass of species i, and the calculation formula is $R_i = R_0/W_i$.

The chemical reaction model used in this paper contains 15 species and 25 reactions [44]. This chemical reaction model is widely used to simulate acetylene-induced oblique detonation [36,37]. The discrete equations in this paper are in AUSMPW + format, which is good for capturing shock waves and obtaining quantitative results [45].

The independence verification of grid resolution is performed in this paper to eliminate the influence of grid resolution on numerical simulation results. Resolution studies in the numerical simulation of two-dimensional (2D) oblique detonation are typically performed with double refinement of the grid size [19]. In this paper, the grid sizes of 0.1 mm * 0.1 mm and 0.2 mm * 0.2 mm are used to simulate the ODW when the position of the transverse jet is L_J = 100 mm and the pressure of the transverse jet is P_0 = 100 KPa. Fig. 4 is the temperature field of the ODW at two grid resolutions. As can be seen in Fig. 4a, there is no difference between the two wave structures, although the picture is slightly clearer at high resolution. Considering the instability of the transverse jet, more precise mesh sizes need to be verified. The grid size of 10 mm near the wall is encrypted to 0.05 mm * 0.05 mm, and the numerical simulation results obtained are shown in Fig. 4b (below). The temperature and pressure curves of the combustion chamber wall are shown in Fig. 5. For comparison, the solid line represents a 0.1 mm * 0.1 mm grid, the dotted line represents a 0.2 mm * 0.2 mm grid, the dash dot line represents a 0.05 mm * 0.05 mm grid, and the T and P are marked on the curve. As shown in Fig. 5, the temperature and pressure curves under the three grid resolutions are only slightly different, indicating that the grid resolution has no effect on the numerical simulation results. As a result, the grid resolution of 0.2 mm * 0.2 mm is used in the numerical simulation in this paper.

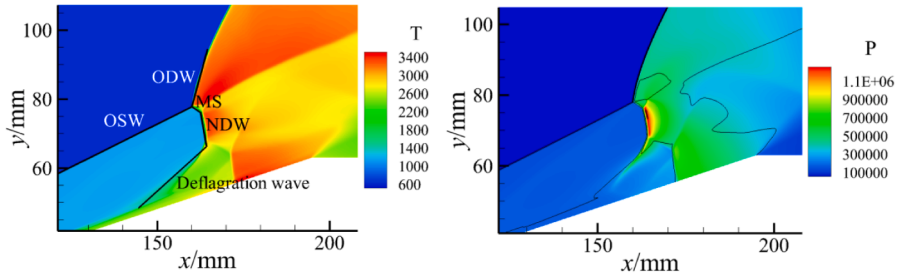

(a)Temperature field (b)Pressure field and iso-Mach line

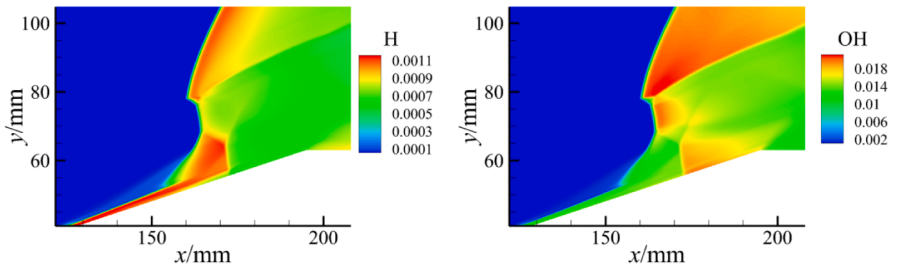

(c)Mass fraction of H radicals (d)Mass fraction of OH radicals

Fig. 7. Specific wave structure of the flow field without transverse jet.

3. Results and discussions

3.1. Effects of transverse jet on ODW

In this section, the effects of the transverse jet on the initiation of ODW are investigated by varying the flow discharge and position of the transverse jet. The first step is to fix the position of the transverse jet to study the influence of the flow discharge of the transverse jet. The position of the transverse jet is at $L_J = 80$ mm, when the pressure of the transverse jet is $P_0 = 100$ KPa, $P_0 = 200$ KPa and $P_0 = 300$ KPa, three wave structures are obtained by simulation. Fig. 6 shows the temperature field of ODW at various conditions. As is shown in Fig. 6, the wave structures of the flow field and the initiation position of the ODW have been changed due to the transverse jet. It has been changed from double Mach interaction (Fig. 6a) to single Mach interaction (Fig. 6b-d). The wave structure changes further as the flow discharge of the transverse jet increases. As the influence of the transverse jet for single Mach interaction, three wave structures are obtained. Fig. 7 to Fig. 10 show the specific wave structures and provide a more detailed analysis of each wave structure.

Fig. 7 shows the specific wave structure of the flow field without transverse jets. As shown in Fig. 7a, when there is no additional transverse jet, the deflagration wave is formed after the induction zone, which further develops into the normal detonation wave (NDW).

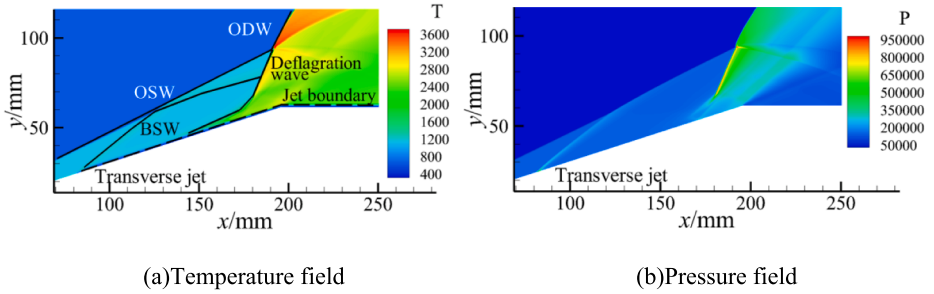

(a)Temperature field (b)Pressure field

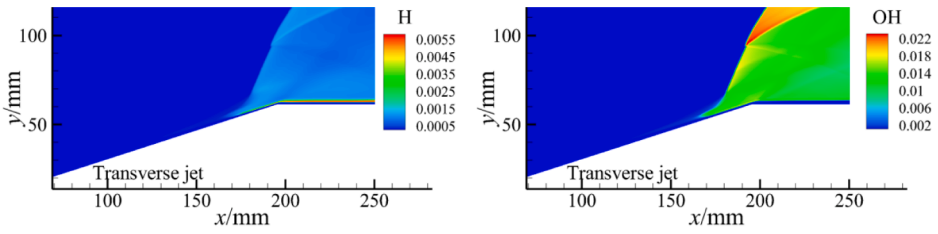

(c)Mass fraction of H radicals (d)Mass fraction of OH radicals

Fig. 8. Specific wave structure of the flow field with transverse jet ($L_J = 80$ mm, $P_0 = 100$ KPa).

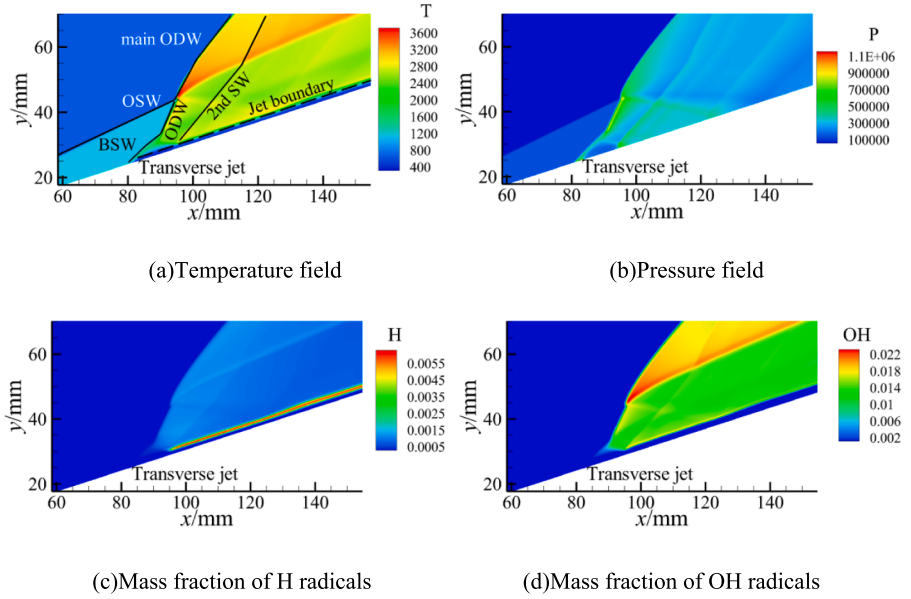

(a)Temperature field (b)Pressure field

(c)Mass fraction of H radicals (d)Mass fraction of OH radicals

Fig. 9. Specific wave structure of the flow field with transverse jet (L_J = 80 mm, P_0 = 200 KPa).

Subsequently, the NDW and the OSW interact to generate the ODW, and the Mach stem (MS) and the slip line (SL) will be generated at the same time. In addition, the interaction of the NDW and the deflagration wave generates a reflected shock wave that produces an irregular reflection at the downstream wall and generates second NDW, resulting in a sudden temperature rise at approximately × = 175 mm. Fig. 7b shows the pressure field and *iso*-Mach line, where an increase in pressure and a decrease in Mach number behind the compression wave is observed. The mass fractions of H radicals and OH radicals are plotted in Fig. 7c and Fig. 7d. The higher mass fraction of H radicals, the lower mass fraction of OH radicals behind the deflagration wave and MS, it indicates that the initiation of chemical reactions and fuel consumption occur more slowly behind the deflagration wave and MS. The lower mass fraction of H radicals but higher mass fraction of OH radicals behind NDW indicates that the initiation of chemical reactions and fuel consumption occur more rapidly behind NDW, resulting in higher consumption of H radicals and generation of OH radicals. The mass fractions of H radicals and OH radicals are both larger behind ODW, indicating that the chemical reaction initiation and fuel consumption are the fastest behind ODW, resulting in the generation of large amounts of H and OH radicals.

The first wave structure of the ODW is the classical wave structure: the non-reactive OSW induced by the front wall of the combustor interacts with the deflagration wave to produce the ODW. Fig. 8 is the specific wave structure of the flow field with transverse jets at L_J = 80 mm and P_0 = 100 KPa. As Fig. 8a presents, since the transverse jet can be treated as a fluidic obstacle, a BSW is formed in front of the transverse jet. As the BSW is weaker enough and no shock-induced combustion occurs. In this situation, the deflagration wave is formed on the jet

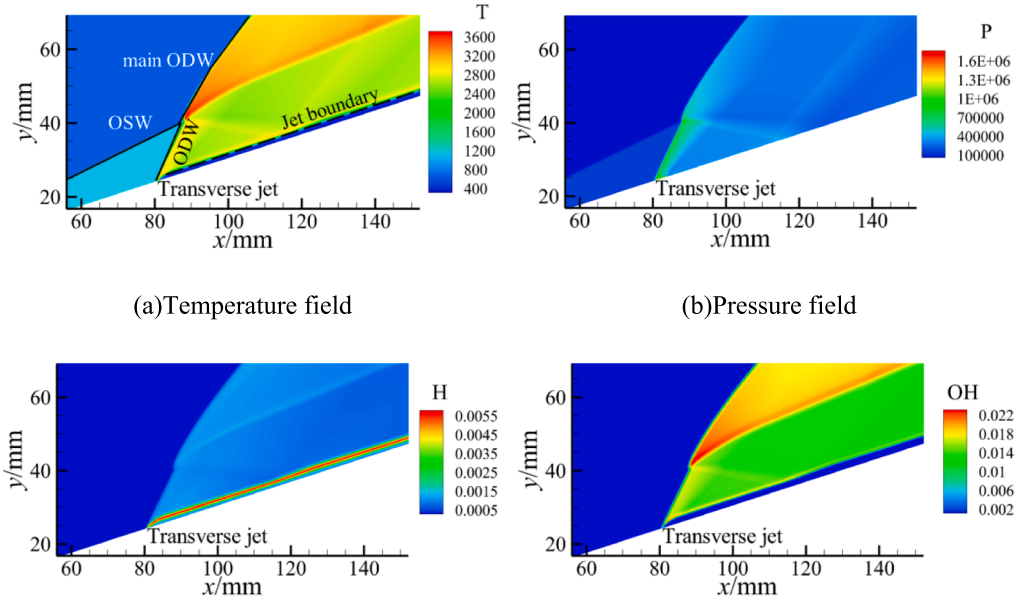

(a)Temperature field (b)Pressure field

(c)Mass fraction of H radicals (d)Mass fraction of OH radicals

Fig. 10. Specific wave structure of the flow field with transverse jet (L_J = 80 mm, P_0 = 300 KPa).

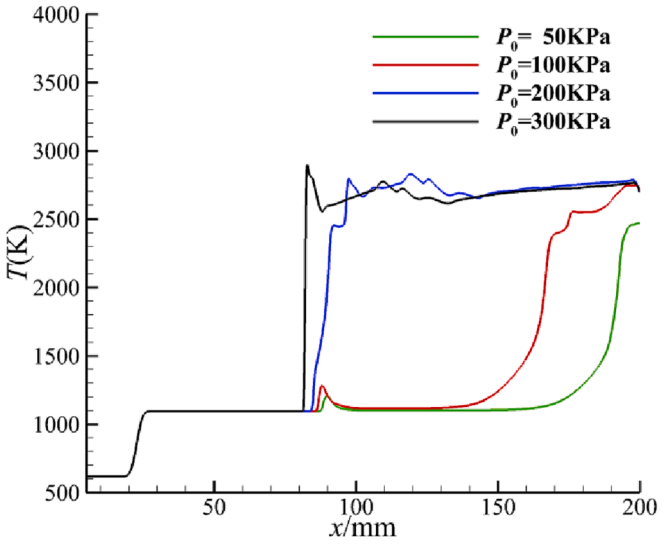

Fig. 11. Temperature curve at a distance of 3 mm from the wall at $L_J = 80$ mm.

boundary, and the downstream of the deflagration wave is coupled with the OSW to form the ODW. Currently, the ODW is induced by the action of the OSW and the deflagration wave, which is consistent with the ODW induced by the wedge. This initiation method is affected by the coupling position of the deflagration wave and the OSW. The difference in the flow discharge of the transverse jet leads to the difference in the momentum. The initiation position of the ODW moves downstream as the flow discharge of the transverse jet decreases. In addition, due to the high flow velocity of the OSW afterward, the transverse jet cannot penetrate the main flow, and a jet boundary is formed near the wall boundary. Fig. 8b shows the pressure field, a clear BSW was generated in front of the transverse jet, and the pressure increased slightly behind the BSW, but the pressure did not continue to increase because the BSW does not induce combustion. Fig. 8c and Fig. 8d show the mass fractions of H radicals and OH radicals, and the type of flame structure produced by deflagration can be observed as a V-shaped flame structure from the mass fraction variation [46–48].

The second wave structure appeared as the flow discharge of the transverse jet increased. Fig. 9 is the specific wave structure of the flow field when the nozzle position of the transverse jet $L_J = 80$ mm and the pressure of the transverse jet $P_0 = 200$ KPa. As Fig. 9a shows, compared with the previous case, the transverse jet can be treated as a fluidic obstacle and a BSW is produced in front of it. However, when the pressure of the transverse jet is increased to a certain extent, the BSW

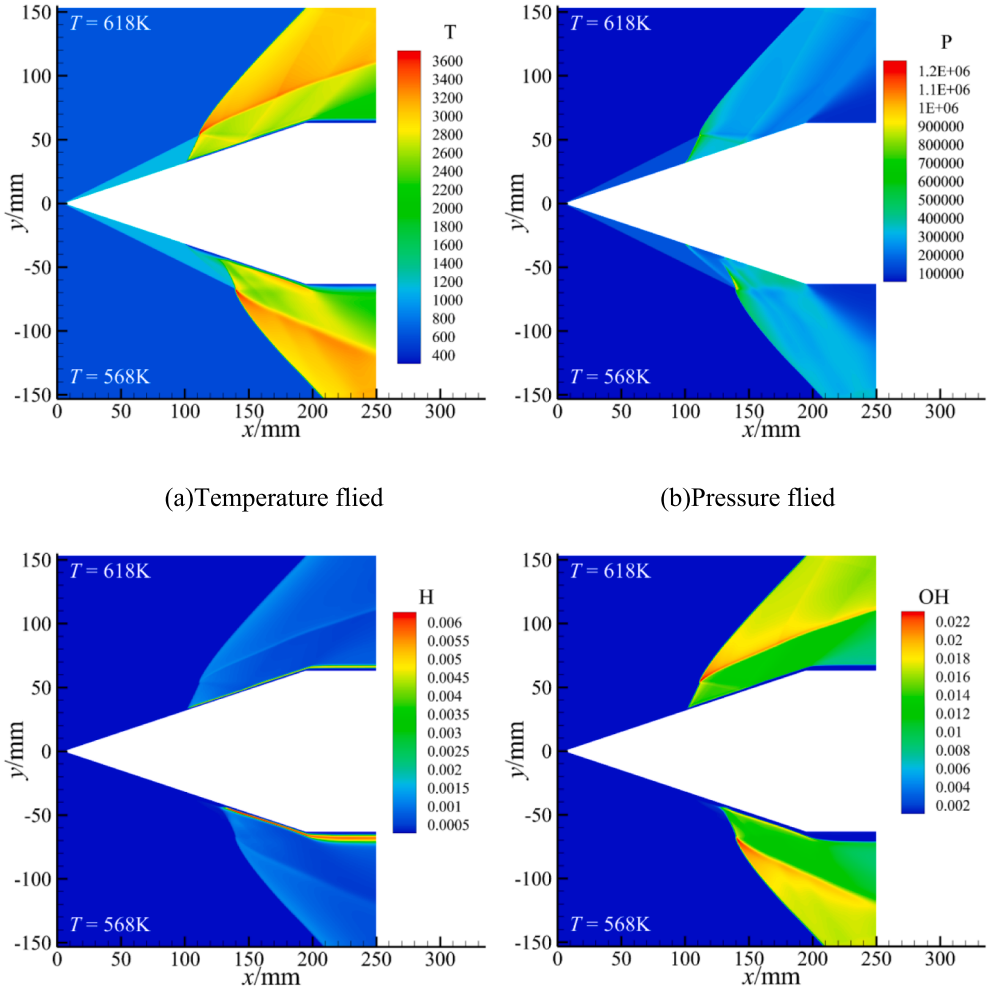

(a)Temperature flied (b)Pressure flied

(c)Mass fraction of H radicals (d)Mass fraction of OH radicals

Fig. 12. Comparison simulation with different temperatures ($L_J = 100$ mm, $P_0 = 200$ KPa).

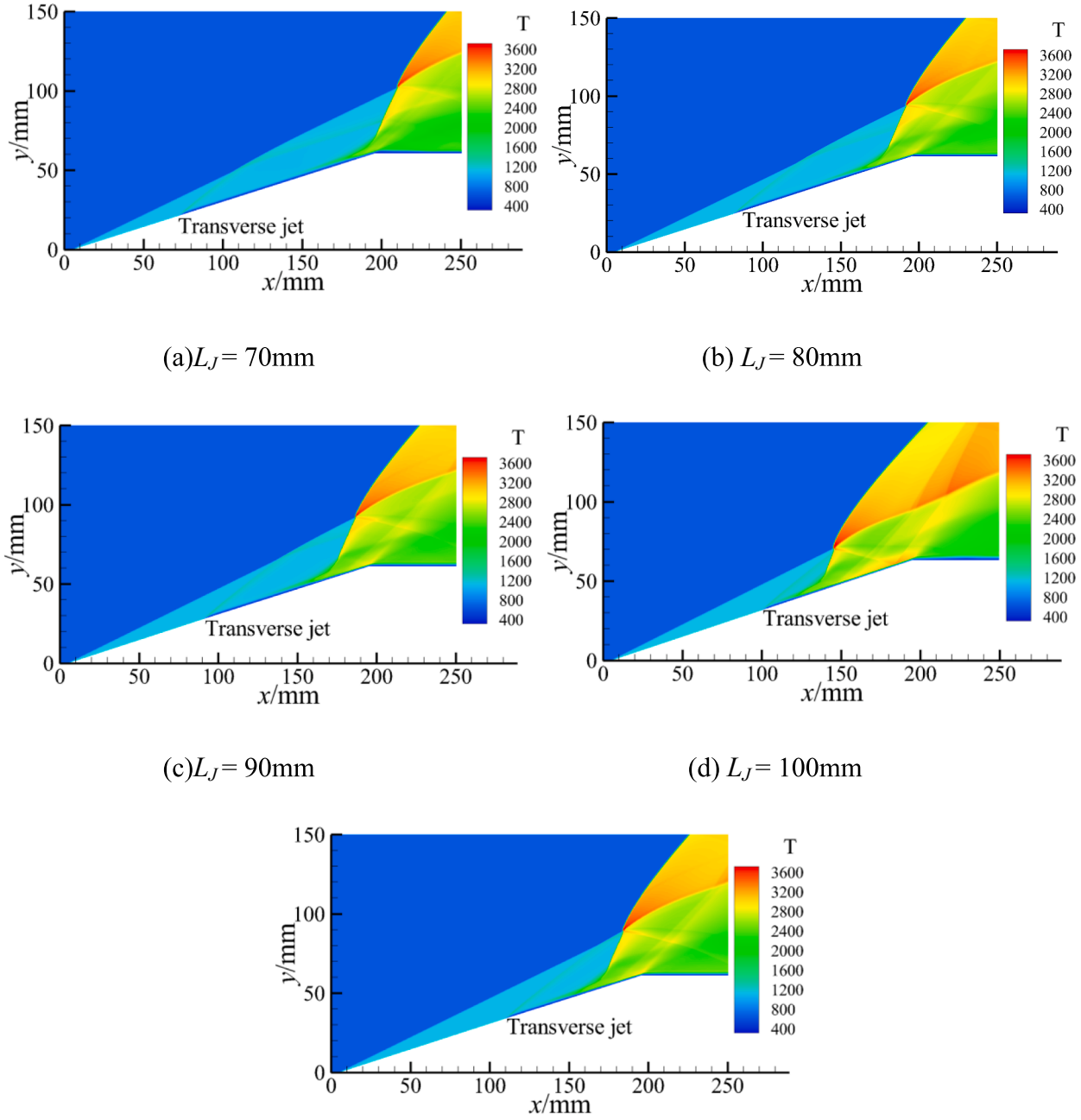

Fig. 13. Temperature field of ODW with transverse jet at P_0 = 100 KPa.

generated in front of the transverse jet is enough large to ignite the combustion, it is different from the previous results. The BSW rapidly develops into ODW and intersects with the main OSW to produce the main ODW. Due to the momentum of the transverse jet being large enough, the generated OSW directly induces combustion. Furthermore, the jet boundary is formed behind the transverse jet, and a 2nd shock wave (2nd SW) is obtained on the jet boundary. The pressure field is shown in Fig. 9b. Due to the rapid development of BSW into ODW, the pressure rises significantly behind ODW, but there is a clear low pressure zone behind BSW. Fig. 9c and Fig. 9d show the mass fractions of H radicals and OH radicals, no significant species change behind BSW, while the species change rapidly behind OSW, indicating that the excitation and combustion are coupled, i.e. this OSW is ODW. In addition, the higher mass fraction of OH radicals behind the main ODW indicates that the combustion behind the main ODW produced by the interaction of OSW and ODW is more aggressive.

The wave structure of the ODW becomes the third one as the flow discharge of the transverse jet continues to increase and become large enough. Fig. 10a is the enlarged wave structure of flow field. When the flow discharge of the transverse jet is large enough, ODW is directly generated in front of the transverse jet. Subsequently, the ODW and OSW intersect to generate the main ODW. It indicates that the formation of the main ODW can be accelerated when the momentum of the transverse jet is large enough. The jet boundary is still present behind the transverse jet at this time, but no other waves are generated on the jet boundary in comparison to the second wave structure. Fig. 10b shows

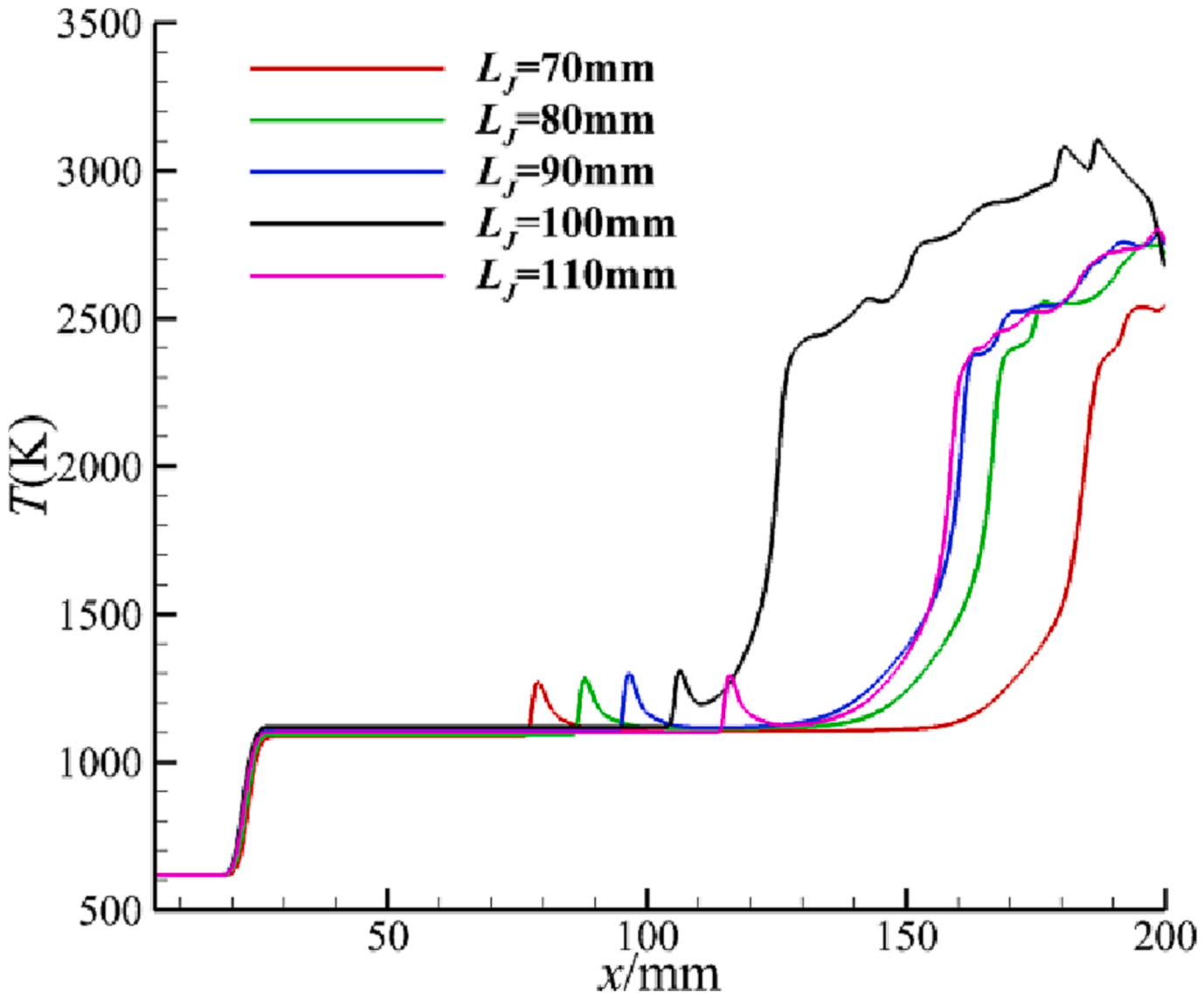

Fig. 14. Temperature curve at a distance of 3 mm from the wall at $P_0 = 100$ KPa.

the pressure field. Compared with Fig. 9b, there is no obvious BSW in front of the transverse jet, and the low pressure zone behind the BSW is disappear. The mass fractions of H radicals and OH radicals are shown in Fig. 10c and Fig. 10d. The species change significantly at the transverse jet, indicating that the combustion initiates behind the ODW induced by the transverse jet.

As the flow discharge of the transverse jet increases, the locations where the chemical reaction occurs move upstream in the three types of wave structures. As shown in Fig. 11, the temperature curves at 3 mm from the wall are extracted. When there is the first wave structure ($P_0 =$ 50 KPa and $P_0 = 100$ KPa), as the positions of the deflagration wave are further downstream, the positions where the chemical reaction occurs are further downstream. The flow discharge of the transverse jet also has a significant impact on the position of the deflagration wave. In the second wave structure ($P_0 = 200$ KPa), the OSW generated in front of the transverse jet induces combustion, and the temperature rises rapidly after the OSW. In the third wave structure ($P_0 = 100$ KPa), the temperature jumps to the maximum within a short distance. This is because the ODW is generated directly in front of the transverse jet, and the combustion induced by ODW is supersonic combustion.

Fig. 12 shows the flow field of ODW at the temperature $T = 568$ K. Fig. 12a shows the temperature field, as the initial temperature decreases, the wave structure of the flow field changes from the second wave structure (BSW - ODW to main ODW) to the first wave structure (deflagration wave to ODW). Suggesting that self-ignition plays a role in the change of wave structure to some extent. Fig. 12b shows the pressure field, the BSW does not induce combustion after lowering the temperature, and the pressure behind the wave surface is smaller. Fig. 12c and Fig. 12d show the mass fractions of H radicals and OH radicals, obviously the position of initiation of combustion is more forward for shock wave induced combustion. The mass fractions of radicals behind the wave surface are similar for different wave structures, indicating that the wave structure has less influence on the intensity of combustion.

The second step is to keep the flow discharge of the transverse jet unchanged and change the position of the transverse jet. In this study, a total of five nozzle positions of transverse jet are set: $L_J = 70$ mm, $L_J =$ 80 mm, $L_J = 90$ mm, $L_J = 100$ mm and $L_J = 110$ mm. Since the characteristic length of the induction zone cannot be obtained on the wall due to the transverse jet, the influence of the transverse jet on the initiation position of the ODW is compared by the L_S defined in Section 2.

Keeping the pressure of the transverse jet remain at $P_0 = 100$ KPa and changing the position of the transverse jet. The results are shown in Fig. 13, as the position of the transverse jet moves downstream from L_J

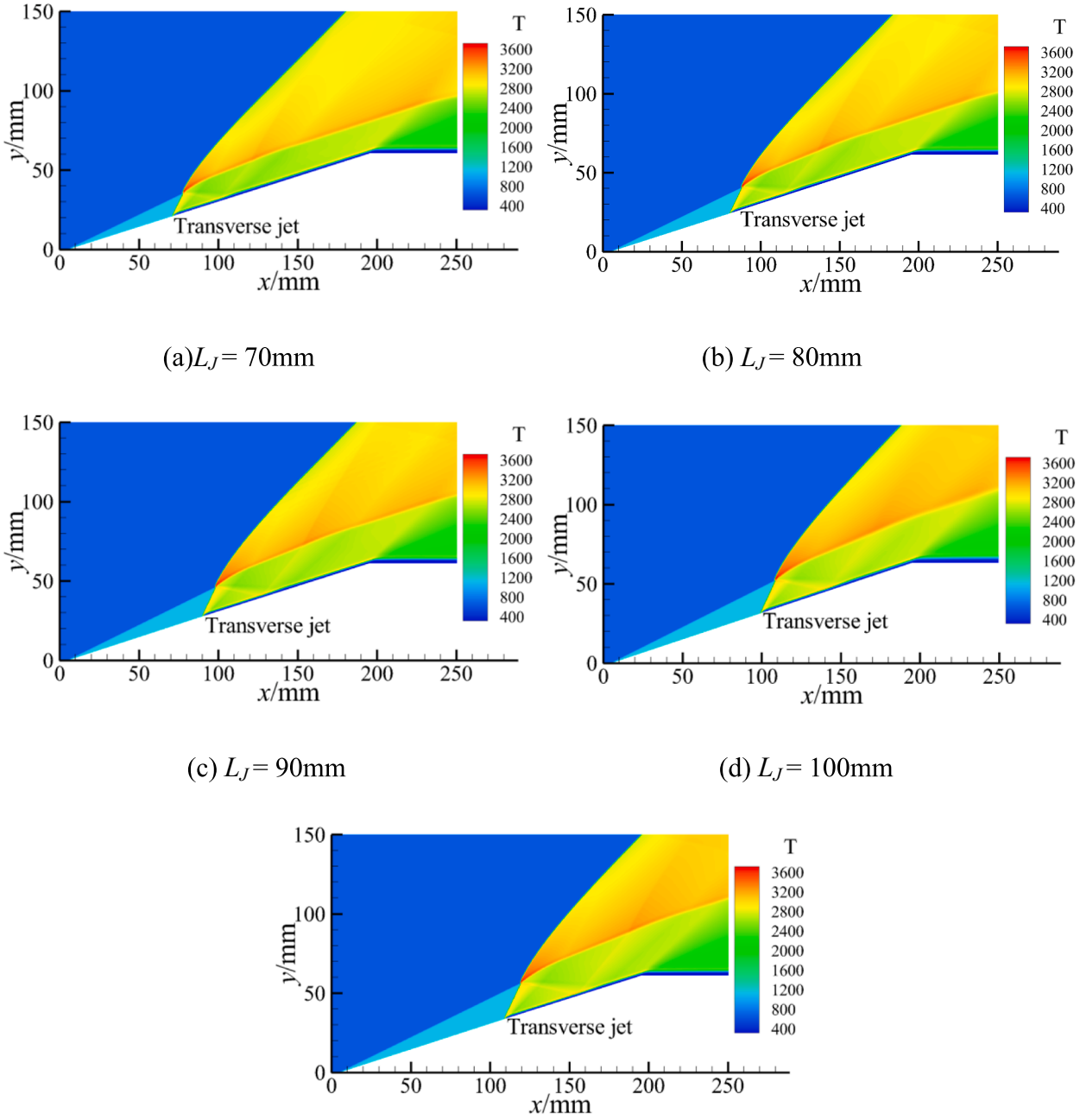

(a)L_J = 70mm (b) L_J = 80mm

(c) L_J = 90mm (d) L_J = 100mm

(a) L_J = 110mm

Fig. 15. Temperature field of ODW with transverse jet at P_0 = 300 KPa.

= 70 mm to L_J = 100 mm, the initiation position of the ODW moves upstream. When the position of the transverse jet continues to move downstream to L_J = 110 mm, the initiation position of the ODW moves downstream. This trend of the ODW initiation position indicates that when the flow discharge of the transverse jet is small and the ODW is generated by the i the DDT transition, there is a particularly suitable location for the transverse jet to initiate the ODW. The same conclusion can be obtained when the pressure of the transverse jet is P_0 = 50 KPa.

Extracting the temperature curve from the temperature contour at 3 mm beyond the wall, the temperature changes as the position of the transverse jets are changed. In Fig. 14, due to the influence of transverse jets, the temperature curves rise slightly and then decrease. The chemical reactions begin as soon as the deflagration wave is generated, and the temperature rises dramatically. In addition, when the position of the transverse jet is L_J = 100 mm, the temperature curve begins to rise earlier. As the position of the transverse jet moves forward or backward, the upward trend of temperature curve moves rearward. This change demonstrates that there is an optimal position of transverse jet in this wave structure. This is consistent with the conclusion of Fig. 13.

When the pressure of the transverse jet is increased to P_0 = 300 KPa, the temperature field of the third wave structure is obtained in Fig. 15. As shown in Fig. 15, when the flow discharge of the transverse jet is large enough, ODW is generated in front of the transverse jet. Since the ODW and the OSW intersect at a point to generate the main ODW, the detonation position of the main ODW is linearly related to the position of the nozzle of the transverse jet. This result indicates that the position of the

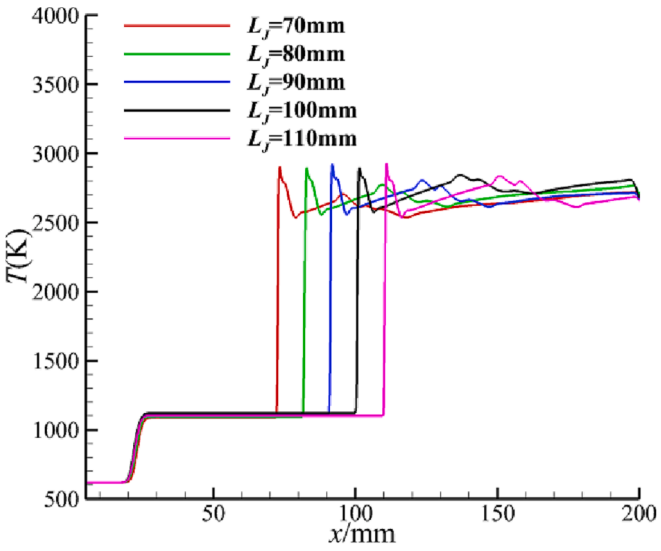

Fig. 16. Temperature curve at a distance of 3 mm from the wall at P_0 = 300 KPa.

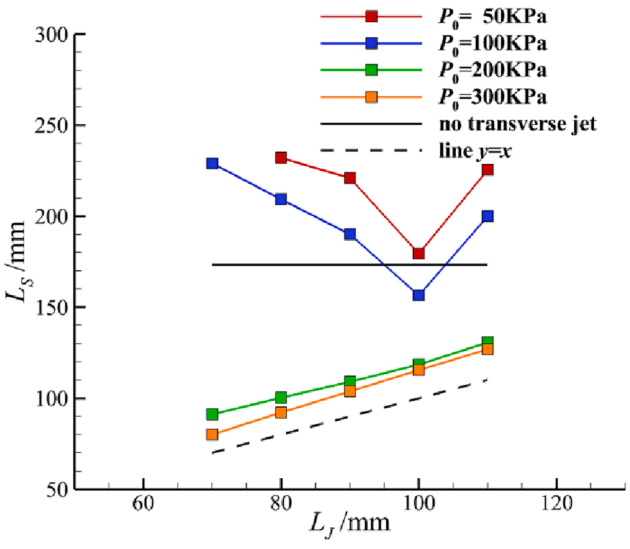

Fig. 17. L_S - L_J relationship diagram.

transverse jet plays a dominant role in the initiation of the ODW when the flow discharge of the transverse jet is large enough. In the same way, when the pressure of the transverse jet is P_0 = 200 KPa, the initiation position of the ODW is also linearly related to the position of the transverse jet nozzle.

Fig. 16 is the temperature curve at 3 mm from the wall at P_0 = 300 KPa. As shown in Fig. 16, since the ODW in front of the transverse jet induces supersonic combustion, the temperature curves quickly rise to the maximum temperature. And the position where the temperature curve rises is positively correlated with the position of the transverse jet. The changing trend of temperature and the analytical results of the temperature field are consistent.

To represent the relationship more intuitively between the initiation position of the ODW and the transverse jet position, the L_S and the corresponding L_J in the same coordinate system are given in Fig. 17. As shown in Fig. 17, the four colored polylines represent the correspondence between the position of the transverse jet L_J and the initiation position L_S of the ODW under different pressures of the transverse jet. The solid black line is the detonation position of the ODW when there is no transverse jet, and the dashed black line is the straight-line representing $y = x$. When the pressures of the transverse jet are P_0 = 50 KPa and P_0 = 100 KPa, the value of L_S first decreases and then increases with the increase of L_J, and the relationship between the L_S and L_J is a U-shaped curve. There is a minimum value of L_S within a certain range, indicating that there is a theoretically most suitable position when the flow discharge of the transverse jet is small. Furthermore, compared to the results without the transverse jet, the initiation distance of ODW is shortened in only a few cases. This shows that when the flow discharge of the transverse jet is small, it may not necessarily accelerate the detonation of the ODW. When the pressures of the transverse jet are P_0 = 200 KPa and P_0 = 300 KPa, the value of L_S increases with the increase of L_J. And the change trend of L_S and L_J is close to y = x, indicating that the correlation between L_S and L_J is a positive correlation.

3.2. Viscous effects on ODW

In the flow of real gases, the effect of viscosity cannot be ignored. Viscosity causes boundary layers to develop on the walls in hypersonic flight. Numerical simulation results show that the viscosity leads to the creation of the boundary layer, which increases the temperature near the wall. Fig. 18 shows the specific wave structure of the flow field under viscous conditions. In Fig. 18, the boundary layer is generated on the wall in front of the transverse jet, but the wave structure does not change and remains the three wave structures in Section 3.1. However, the increase in temperature results in a decrease in the flow discharge required for wave structure transformation. In viscous conditions, when the pressure of the transverse jet is P_0 = 100 KPa, the wave structure changes from the first to the second. When the pressure of the transverse jet is P_0 = 200 KPa, the wave structure changes from the second to the third.

Fig. 19 shows the correspondence between L_S and L_J in viscous conditions. When the pressure of the transverse jet is P_0 = 50 KPa, L_S first decreases and then increases with the change of L_J, and the change trend of the curve is a U-shaped curve. When the pressure of the transverse jet increases to P_0 = 100 KPa, L_S still increases first and then decreases. However, when the position of the transverse jet is L_J = 90 mm, L_J = 100 mm and L_J = 110 mm, at this time, L_S and L_J are positively correlated. From the above analysis, this is because the viscosity has changed the wave structure. When the pressure of the transverse jet is P_0 = 200 KPa and P_0 = 300 KPa, the value of L_S increases with the increase of L_J. And the change trend of L_S and L_J is close to the line that expresses y = x, indicating that the correlation between L_S and L_J is a positive correlation. This is consistent with the previous analysis results.

For the transverse jet with low pressure, the viscosity has a significant influence on the wave structure. In Fig. 20, for lower pressure at P_0 = 50 KPa and P_0 = 100 KPa, the detonation distance is obviously affected by the viscosity. The viscous boundary layer increases the temperature near the wall, and the position of the deflagration wave moves upstream at the first wave structure. The increase in temperature also causes the second wave structure to appear earlier, resulting in a further acceleration of the detonation distance. For higher pressures at P_0 = 200 KPa and P_0 = 300 KPa, the viscous boundary layer also accelerates the transition from the second wave structure to the third wave structure. Since the initiation positions of these two wave structures are close to the position of the transverse jet, the viscous boundary layer moves the initiation positions slightly forward.

4. Summary and conclusions

In this paper, the effects of the transverse jet on the initiation characteristics of ODW are investigated by solving two-dimensional multi-component Navier-Stokes equations considering chemical reactions. The following conclusions are drawn from the analysis and discussion of the numerical simulation results:

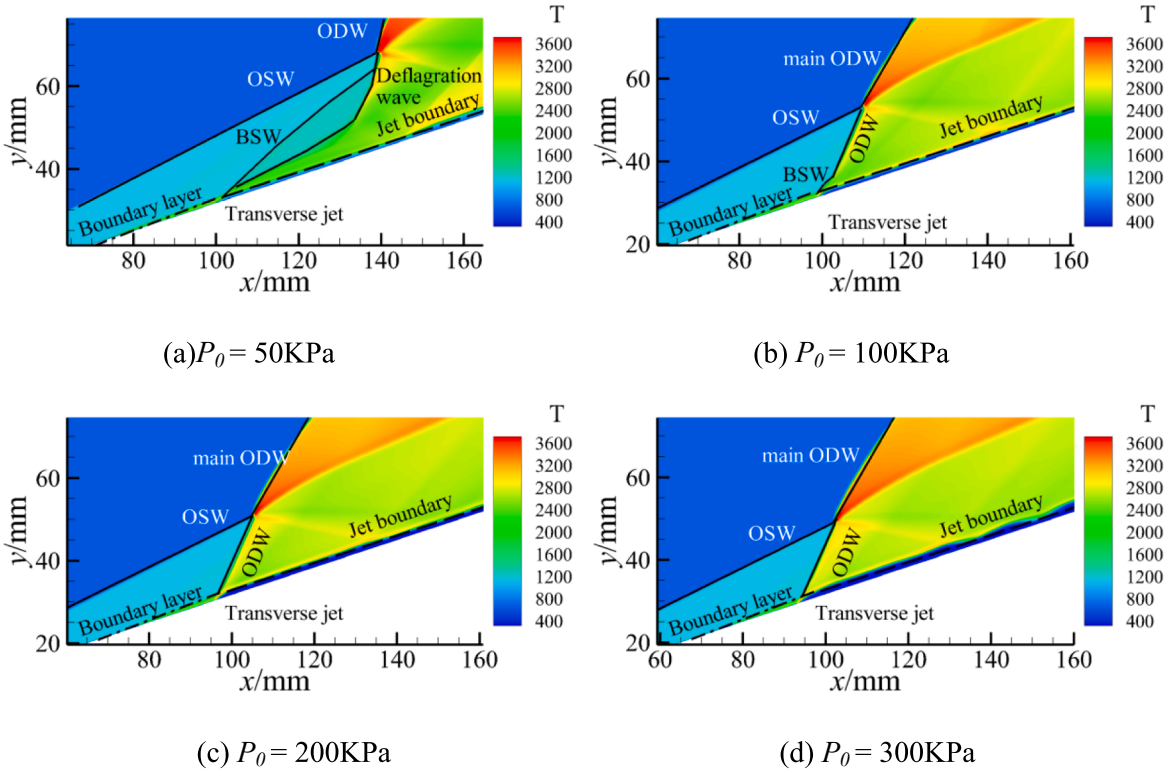

(a)P_0 = 50KPa (b) P_0 = 100KPa

(c) P_0 = 200KPa (d) P_0 = 300KPa

Fig. 18. Specific wave structure of the flow field with transverse jet (L_J = 100 mm).

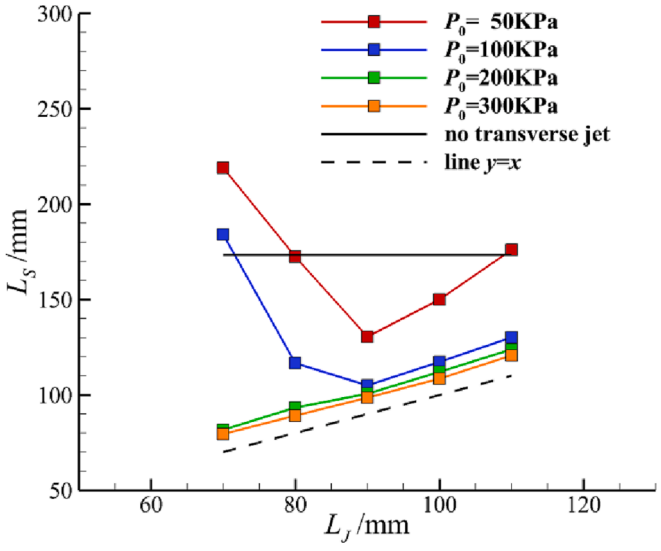

Fig. 19. L_S-L_J relationship diagram.

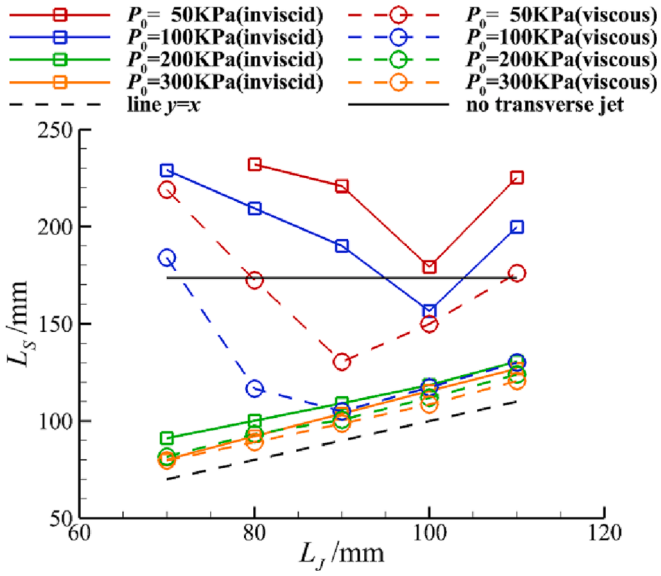

Fig. 20. Comparison of inviscid results and viscous results.

(1) The addition of the transverse jet will change the original wave structure of the ODW. And according to the flow discharge of the transverse jet, three wave structures will be generated: First, like the wedge-induced ODW, the wave structure mainly includes OSWs, deflagration waves, and ODWs. Second, BSWs are generated before the transverse jet and rapidly develop into ODWs. The wave structure mainly includes BSWs, ODWs, OSWs, and main ODWs. Third, ODWs are generated directly before the transverse jet, and the wave structure mainly includes ODWs, main OSWs, and main ODWs.

(2) The initiation of the ODW is affected by the position of the transverse jet. When the flow discharge of the transverse jet is small, the detonation distance of the ODW is longer, and the relationship between the detonation distance and the position of the transverse jet is a U-shaped curve. The detonation distance of the ODW is shorter when the flow discharge of the transverse jet is large, and the detonation distance is positively correlated with the position of the transverse jet.

(3) If the viscous effect is considered, the viscous boundary layer is created on the wall. The boundary layer increases the temperature near the wall and accelerates the generation of deflagration waves, OSWs, and ODWs near the transverse jet in the above three wave structures. And it can accelerate the transformation of

three wave structure and shorten the initiation distance of oblique detonation.

In this paper, the accelerated initiation of ODW is achieved by adding a hydrogen jet. The initiated position of the ODW and the jet position are positively correlated at high flow discharges, which is a good way to achieve the goal of accelerating the initiation of the ODW in the desired position. And compared to the ODW induced by blunt bump, the hydrogen jet also avoids losses due to thermal damage. Of course, like the problems encountered with blunt bump-induced ODW, the resistance caused by the hydrogen jet is also a pressing issue.

CRediT authorship contribution statement

Zhang Yichen: Data curation, Writing – original draft, Software. **Xiang Gaoxiang:** Writing – review & editing, Conceptualization, Methodology. **Gao Xiang:** Visualization, Investigation. **Yu Jia:** Investigation, Software. **Hu Xiquan:** Investigation, Software. **Xin Yirong:** Supervision, Software, Validation. **Li Danyang:** Supervision, Software, Validation. **Wang Qiu:** Writing – review & editing.

Declaration of Competing Interest

The authors declare the following financial interests/personal relationships which may be considered as potential competing interests: [Zhang Yichen, Xiang Gaoxiang, Gao Xiang,Yu Jia, Hu Xiquan, Xin Yirong, Li Danyang, Wang Qiu].

Data availability

Data will be made available on request.

Acknowledgements

This work is supported by National Natural Science Foundation of China (12202365), the Guangdong Basic and Applied Basic research Foundation (2022A1515011565, 2023A1515010031), Natural Science Foundation of Chongqing (2022NSCQ-MSX5709), Foundation of State Key Laboratory of High Temperature Gas Dynamics (2021KF10), and the China Postdoctoral Science Foundation funded project (2021 M692633, 2022 T150534).

References

[1] Wang K, Teng H, Yang P, et al. Numerical investigation of flow structures resulting from the interaction between an oblique detonation wave and an upper expansion corner. J Fluid Mech 2020;903:A28.
[2] Xiang G, Li H, Cao R, et al. Study on feature of oblique detonation induced by a finite wedge in hydrogen-air mixtures with various equivalence ratio. Fuel 2020;264:116854.
[3] Cai X, Liang J, Deiterding R. Numerical investigation on detonation control using a pulse hot jet in supersonic combustible mixture. Combust Sci Technol 2016;188(10):1674–90.
[4] Huang X, Lin Z. Analysis of coupled-waves structure and propagation characteristics in hydrogen-assisted kerosene-air two-phase rotating detonation wave. Int J Hydrogen Energy 2022;47(7):4868–84.
[5] Jiang Z, Zhang Z, Liu Y, Wang C, Luo C. Criteria for hypersonic airbreathing propulsion and its experimental verification. Chin J Aeronaut 2021;34(3):94–104.
[6] Xiang G, Zhang Y, Tu Q, Gao Y, Huang X, Peng T. The initiation characteristics of oblique detonation waves induced by a curved surface. Aerosp Sci Technol 2022;128:107743.
[7] Yang P, Ng HD, Teng H. Numerical study of wedge-induced oblique detonations in unsteady flow. J Fluid Mech 2019;876:264–87.
[8] Xiang G, Zhang Y, Zhang C, Kou Y. Study on initiation mechanism of oblique detonation induced by blunt bump on wedge surface. Fuel 2022;232:124314.
[9] Fang Y, Hu Z, Teng H. Numerical investigation of oblique detonations induced by a finite wedge in a stoichiometric hydrogen-air mixture. Fuel 2018;234:502–7.
[10] Xiang G, Gao X, Tang W, Xie X, Huang X. Oblique detonation waves induced by two symmetrical wedges in hydrogen-air mixtures. Fuel 2021;295:120615.
[11] Sun M, Zhao Y, Zhao G, et al. A conceptual design of shock-eliminating clover combustor for large scale scramjet engin. Acta Astronaut 2017;130:34–42.
[12] Huang W, Yan L. Numerical investigation on the ram–scram transition mechanism in a strut-based dual-mode scramjet combustor. Int J Hydrogen Energy 2016;41(8):4799–807.
[13] Xiang G, Gao X, Tang W, Jie X, Huang X. Numerical study on transition structures of oblique detonations with expansion wave from finite-length cowl. Phys Fluids 2020;29(5):056108.
[14] Sun M-b, Zhong Z, Liang J-H, Wang H-b. Experimental investigation on combustion performance of cavity-strut injection of supercritical kerosene in supersonic model combustor. Acta Astronaut 2016;127:112–9.
[15] Li C, Kailasanath K, Oran E. Detonation structures behind oblique shocks. Phys Fluids 1994;6(4):1600–11.
[16] Viguier C, Silva LFFd, Desbordes D, Deshaies B. Onset of oblique detonation waves: comparison between experimental and numerical results for hydrogen-air mixtures. Symp (Int) Combust 1996;26(2):3023–31.
[17] Desbordes D, Hamada L, Guerraud C. Supersonic H_2-air combustions behind oblique detonation waves. Shock Waves 1995;4(6):339–45.
[18] Kamel MR, Morris CI, Stouklov IG, Hanson RK. PLIF imaging of hypersonic reactive flow around blunt bodies. Symp (Int) Combust 1996;26(2):2909–15.
[19] Teng H, Jiang Z. On the transition pattern of the oblique detonation structure. J Fluid Mech 2012;713:659–69.
[20] Miao S, Zhou J, Liu S, Cai X. Formation mechanisms and characteristics of transition patterns in oblique detonations. Acta Astronaut 2018;142:121–9.
[21] Yang P, Teng H, Jiang Z, Ng HD. Effects of inflow Mach number on oblique detonation initiation with a two-step induction-reaction kinetic model. Combust Flame 2018;193:246–56.
[22] Liu Y, Wang L, Xiao B, et al. Hysteresis phenomenon of the oblique detonation. Combust Flame 2018;192:170–9.
[23] Fang Y, Hu Z, Teng H, et al. Effects of inflow equivalence ratio inhomogeneity on oblique detonation initiation in hydrogen-air mixtures. Aerosp Sci Technol 2017;71:256–63.
[24] Chen N, Seyed A, Sudip B, et al. Numerical study on effects of equivalence ratio on initiation characteristics of oblique detonation waves. J Propuls Technol 2018;39(12):2798–805.
[25] Qin Q, Zhang X. Study on the effects of geometry on the initiation characteristics of the oblique detonation wave for hydrogen-air mixture. Int J Hydrogen Energy 2019;44(31):17004–14.
[26] Xiang G, Li H, Zhang G, Xie X, Zhang Y. Characteristics of the oblique detonation flow field induced by a complex wave structure. Int J Hydrogen Energy 2021;46(33):17435–45.
[27] Qin Q, Zhang X. Study on the initiation characteristics of the oblique detonation wave by a co-flow hot jet. Acta Astronaut 2020;177:86–95.
[28] Cheng J, Zhang Bo, Liu H, Wang F. The precursor shock wave and flame propagation enhancement by CO_2 injection in a methane-oxygen mixture. Fuel 2021;283:118917.
[29] Wang Z, Zhang Y, Chen X, Liang Z, Zheng L. Investigation of hot jet effect on detonation initiation Characteristics. Combust Sci Technol 2017;189(3):498–519.
[30] Li H, Li J, Xiong C, Fan W, Zhao L, Han W. Investigation of hot jet on active control of oblique detonation waves. Chin J Aeronaut 2020;33(3):861–9.
[31] Wang Z, Pan Z, Huang J, Wei L, Wang Y, Wang Y. Effects of double-jet positions on detonation initiation characteristics. Aerosp Sci Technol 2020;97:105609.
[32] Chen W, Liang J, Cai X, et al. Three-dimensional simulations of detonation propagation in circular tubes: Effects of jet initiation and wall reflection. Phys Fluids 2020;32:046104.
[33] Teng H, Ng HD, Jiang Z. Initiation characteristics of wedge-induced oblique detonation wave in a stoichiometric hydrogen-air mixture. Proc Combust Inst 2017;36:2735–42.
[34] Wang T, Zhang Y, Teng H, Jiang Z, Ng HD. Numerical study of oblique detonation wave initiation in a stoichiometric hydrogen-air mixture. Phys Fluids 2015;27(9):096101.
[35] Li Y, Bi M, Zhang S, Jiang H, Gan Bo, Gao W. Dynamic couplings of hydrogen/air flame morphology and explosion pressure evolution in the spherical chamber. Int J Hydrogen Energy 2018;43(4):2503–13.
[36] Fang Y, Zhang Y, Deng X, et al. Structure of wedge-induced oblique detonation in acetylene-oxygen-argon mixtures. Phys Fluids 2019;31:026108.
[37] Zhang Y, Fang Y, Ng HD, Teng H. Numerical investigation on the initiation of oblique detonation waves in stoichiometric acetylene–oxygen mixtures with high argon dilution. Combust Flame 2019;204:391–6.
[38] Zhang B. Detonation limits in methane-hydrogen-oxygen mixtures: Dominant effect of induction length. Int J Hydrogen Energy 2019;44(41):23532–7.
[39] Zhang B, Liu H, Yan B, Ng HD. Experimental study of detonation limits in methane-oxygen mixtures: Determining tube scale and initial pressure effects. Fuel 2020;259:116220.
[40] Zhang B, Chang X, Bai C. End-wall ignition of methane-air mixtures under the effects of CO_2/Ar/N_2 fluidic jets. Fuel 2020;270:117485.
[41] Zhang B, Liu H, Yan B. Effect of acoustically absorbing wall tubes on the near-limit detonation propagation behaviors in a methane–oxygen mixture. Fuel 2019;236:975–83.
[42] Xi X, Tian C, Wang K. Effects of hydrogen addition on oblique detonations in methaneeair mixtures. Int J Hydrogen Energy 2022;47:8621–9.
[43] McBride BJ, Gordon S, Reno MA. Coefficients for calculating thermodynamic and transport properties of individual species. NASA TM-4513; 1993.
[44] Varatharajan B, Williams FA. Chemical-kinetic descriptions of high-temper-ature ignition and detonation of acetylene-oxygen-diluent systems. Combust Flame 2001;124(4):624–45.
[45] Kim KH, Kim C, Rho OH. Methods for the accurate computations of hypersonic flows: I. AUSMPW+ scheme. J Comput Phys 2001;174(1):38–80.

[46] Iwata K, Nakaya S, Tsue M. Numerical investigation of the effects of nonuniform premixing on shock-induced combustion. AIAA J 2016;54(5):1682–92.
[47] Iwata K, Nakaya S, Tsue M. Wedge-stabilized oblique detonation in an inhomogeneous hydrogen–air mixture. P Combust Inst 2017;36(2):2761–9.
[48] Xiang G, Li X, Sun X, Chen X. Investigations on oblique detonations induced by a finite wedge in high altitude. Aeros Sci Technol 2019;95:105451.